Electronic Supplementary Material (ESI) for Journal of Materials Chemistry A.

Supporting Information
Bimetallic MoNi/WNi Nanoalloys for Ultra-Sensitive Wearable Temperature Sensors

Yuefeng Gu[a], Junyang Hao[b], Tiancheng Wu[b], Zhigang Zhang[b], Zhaoxi Zhang[b], Qiuhong Li[a,b*]

[a] ***School of Electronic Science and Engineering, Xiamen University, Xiamen, 361005, China***

[b] ***Pen-Tung Sah Institute of Micro-Nano Science and Technology, Xiamen University, Xiamen, 361005, China***

Materials

$Ni(NO_3)_2 \cdot 6H_2O$, $(NH_4)_6Mo_7O_{24} \cdot 4H_2O$, $(NH_4)_{10}W_{12}O_{41} \cdot XH_2O$, acetone, and ethanol were purchased from Sinopharm Chemical Reagent $NH_3 \cdot H_2O$ Co., Ltd. $(CH_2OH)_2$ and poly tetra fluoroethylene (PTFE) were purchased from Shanghai Aladdin Bio-Chem Technology Co., Ltd. All reagents were of analytical grade and used as received. Deionized water was used throughout the whole experiment.

DFT calculations

All the computations are evaluated with the plane-wave-based density functional theory (DFT) method as implemented in the Vienna ab initio simulation package (VASP). The model of $MoNi_4$ and WNi_4 are correction treated according to the previous studies, ensuring the reliability and comparability.[1-4] The simulation is run with a cutoff energy of 500 eV throughout the computations and a Gaussian electron smearing of 0.1 eV is used. The convergence criteria for energy and force are 10^{-5} eV and 0.02 eV/Å, respectively.

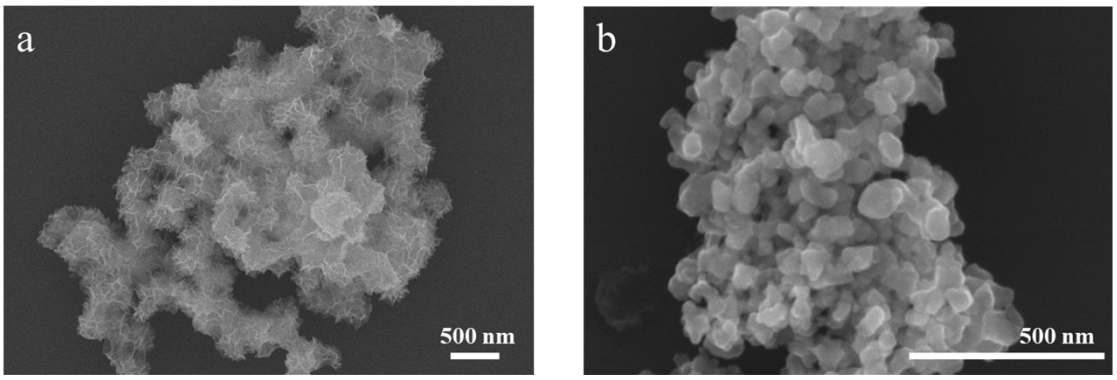

Figure S1. SEM images of (a) $MoNi_4$ and (b) WNi_4.

a

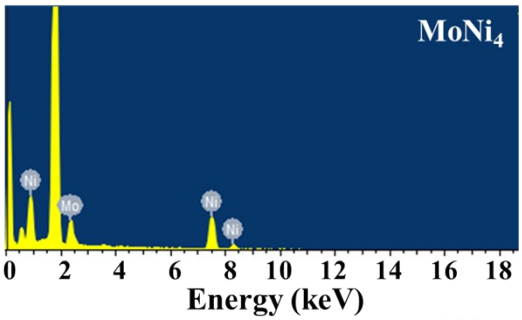

Element	Weight %	Atomic %
Ni K	69.71	79.70
Mo K	30.29	20.30

b

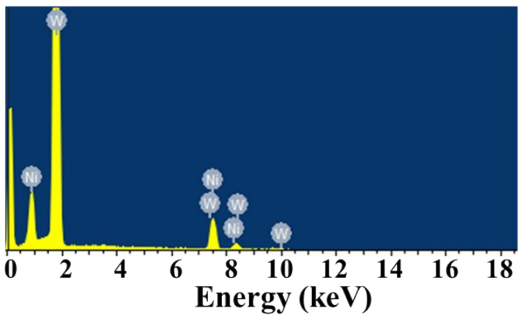

Element	Weight %	Atomic %
Ni K	71.10	81.29
W K	28.90	18.71

Figure S2. EDS spectra of (a) MoNi4 and (b) WNi4 and their atomic components.

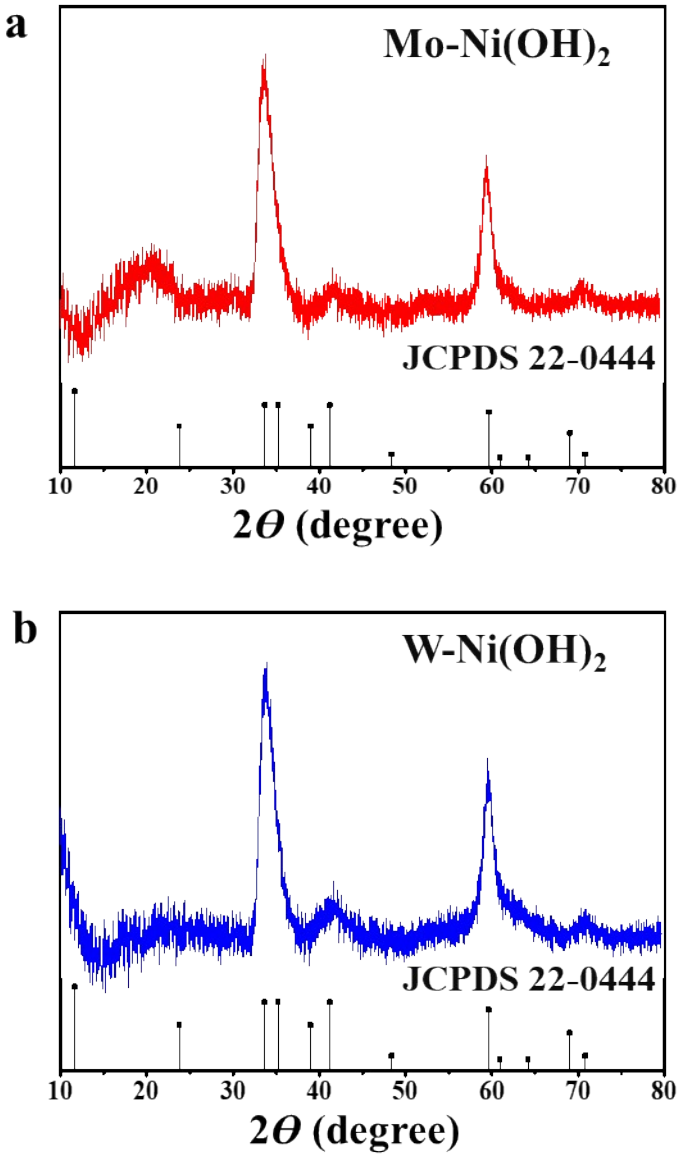

Figure S3. XRD patterns of (a) Mo doped $Ni(OH)_2$ (Mo-$Ni(OH)_2$) and (b) W doped $Ni(OH)_2$ (W-$Ni(OH)_2$).

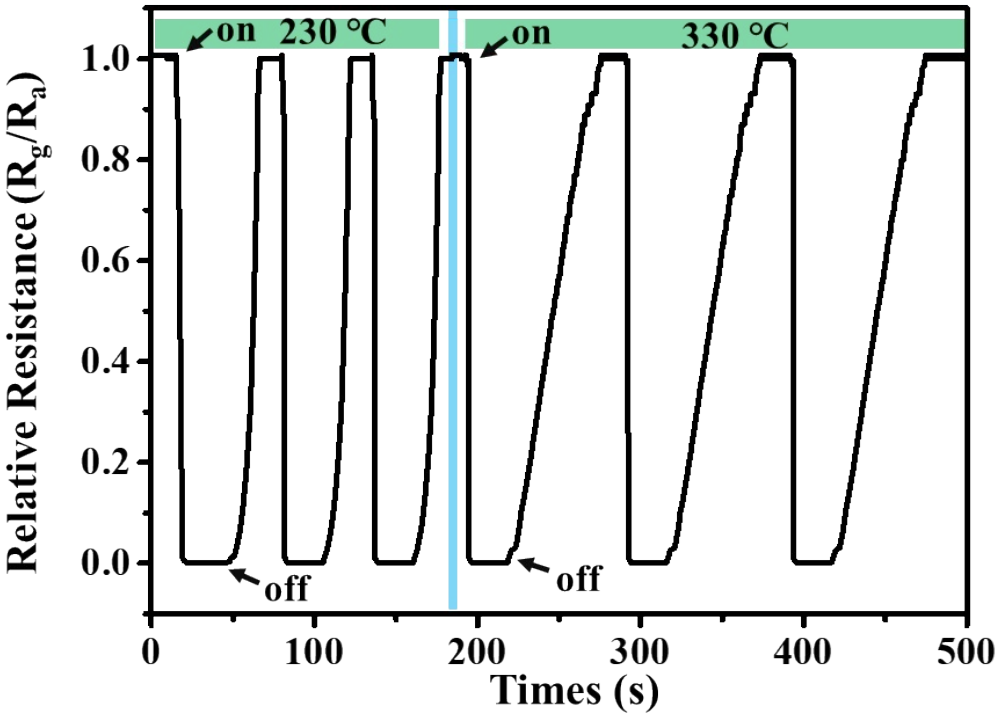

Figure S4. Continuous dynamic response of WNi_4 sensor to 230 and 330 ℃.

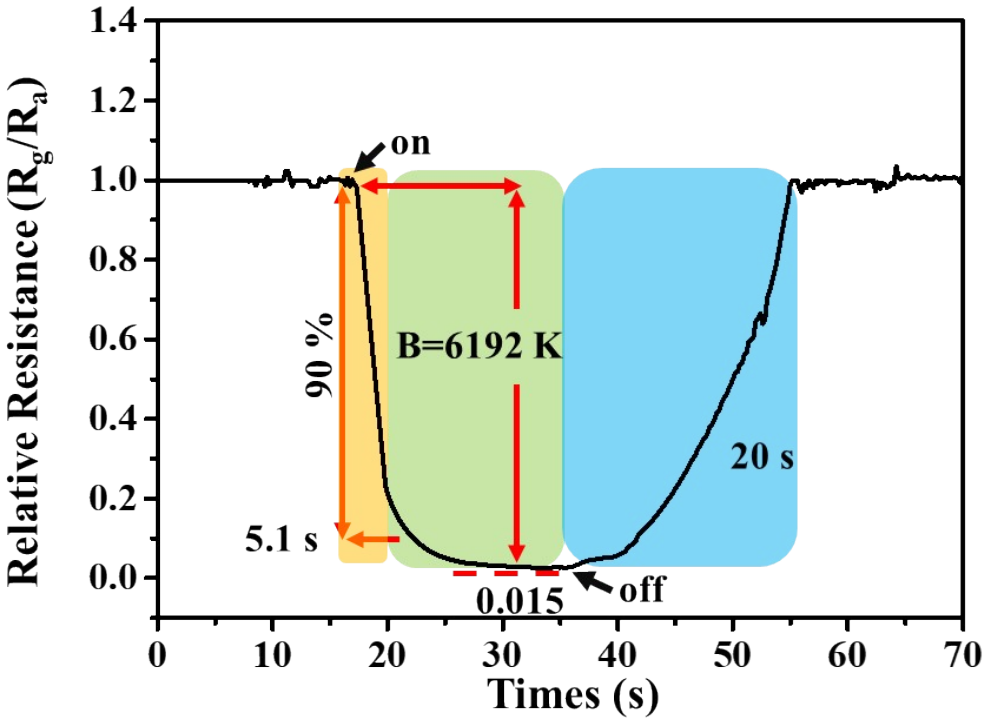

Figure S5. Dynamic response of WNi_4 sensor for testing range (25-100 ℃).

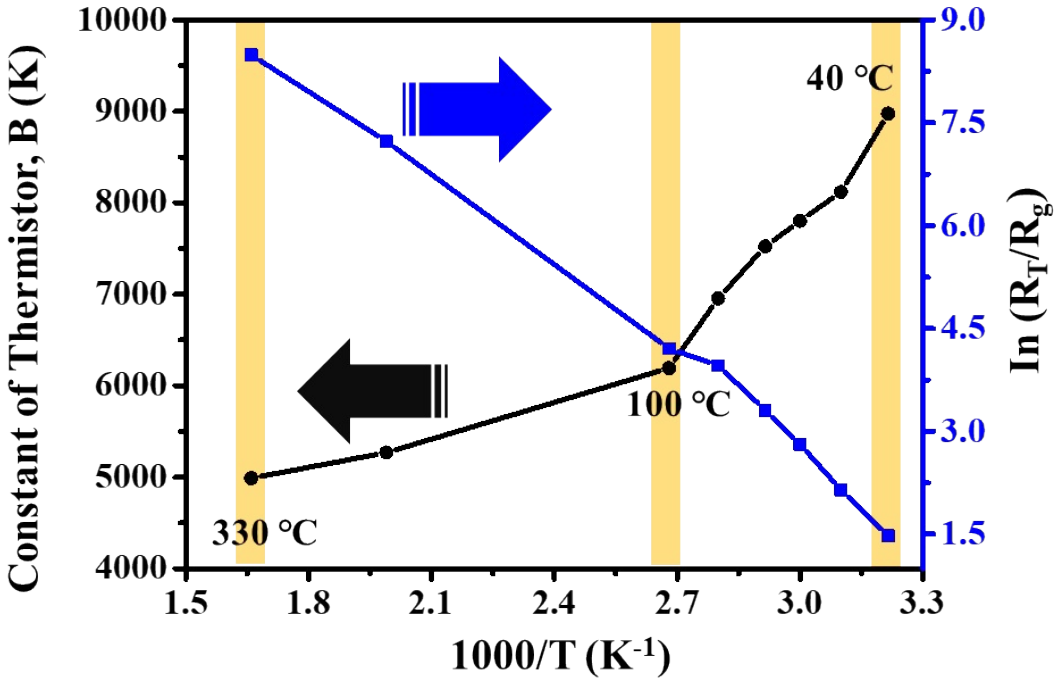

Figure S6. Constant of thermistor (B-value) and resistance ratio (R_T/R_g) of WNi_4 temperature sensor from 40-330 ℃.

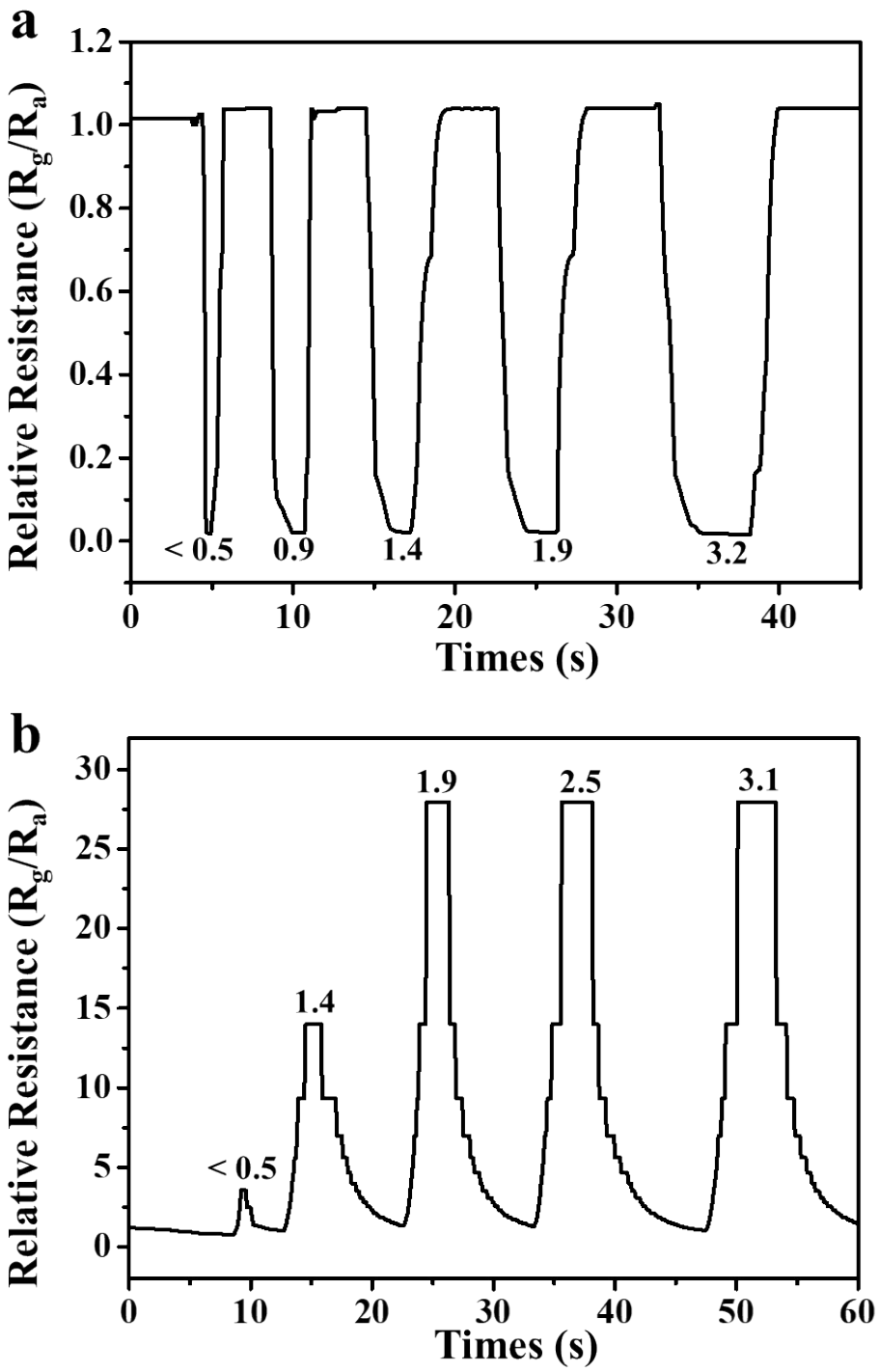

Figure S7. Dynamic response of the $MoNi_4$ sensor at (a) room temperature, and (b) 230 ℃.

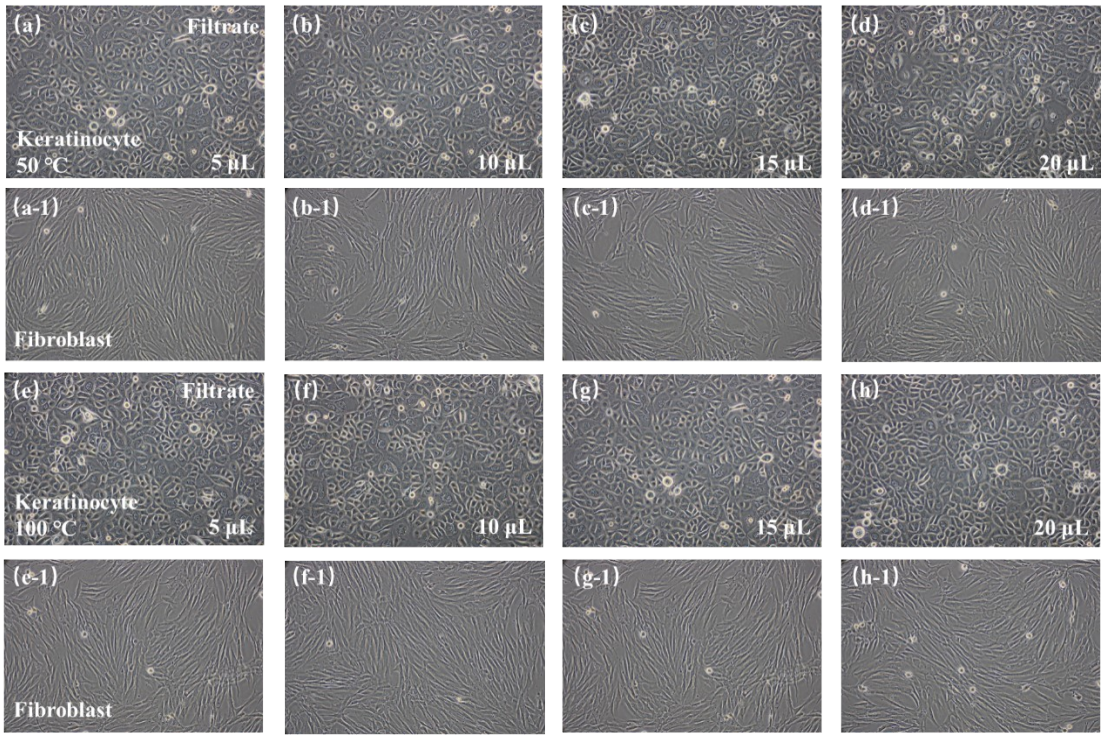

Figure S8. Cell proliferation experiment for biocompatibility study. The filtrate is added into DMEM with different doses for 72 h. 50 ℃ treatment of (a) and (a-1) 5 μL, (b) and (b-1) 10 μL, (c) and (c-1) 15 μL, (d) and (d-1) 20 μL. 100 ℃ treatment of (e) and (e-1) 5 μL, (f) and (f-1) 10 μL, (g) and (g-1) 15 μL, (h) and (h-1) 20 μL.

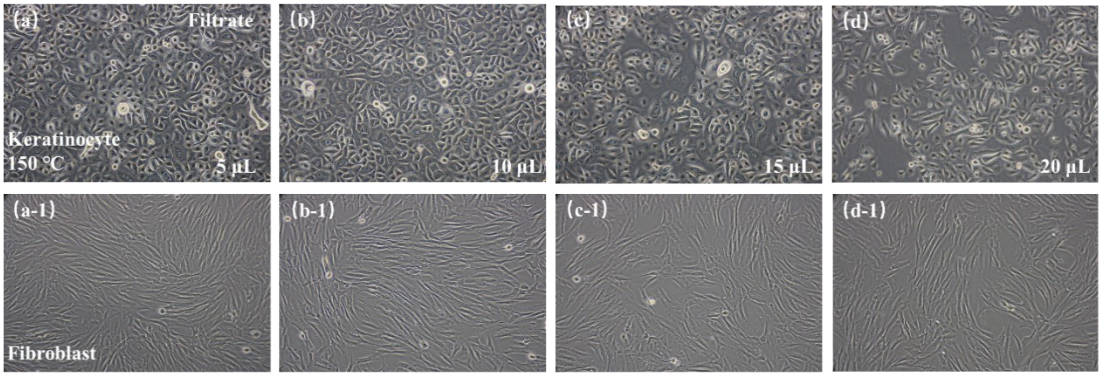

Figure S9. Cell proliferation experiment for biocompatibility study. The filtrate treated at 150 ℃ is added into DMEM with different doses for 72 h. (a) and (a-1) 5 μL, (b) and (b-1) 10 μL, (c) and (c-1) 15 μL, (d) and (d-1) 20 μL.

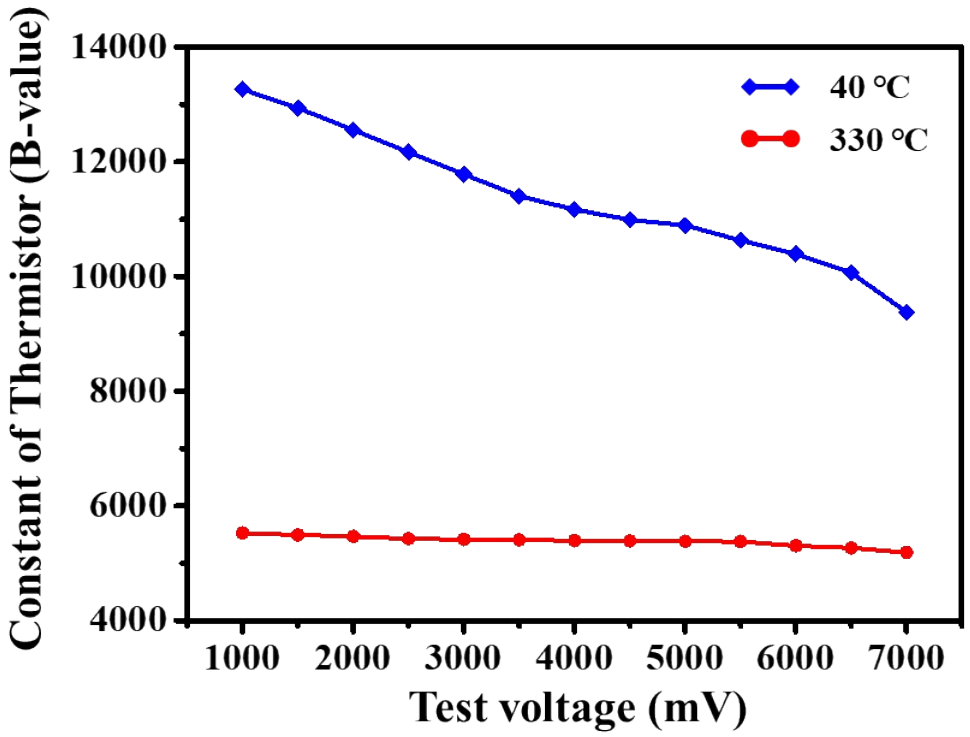

Figure S10. Constant of thermistor (B-value) of $MoNi_4$ sensor at different test voltages.

Figure S10 shows the decreasing tendency of B-value with test voltage at low or high temperatures. The increasing voltage could make electronic detrapping and motion easier, causing the decrease of Ea.

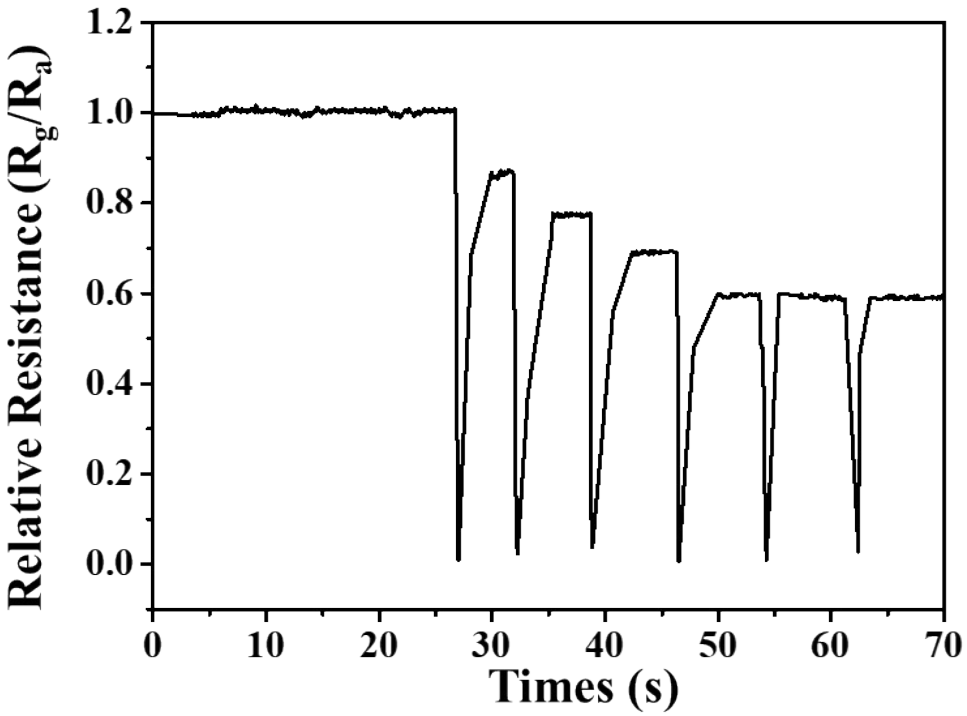

Figure S11. Continuous exhale test of $MoNi_4$ sensor.

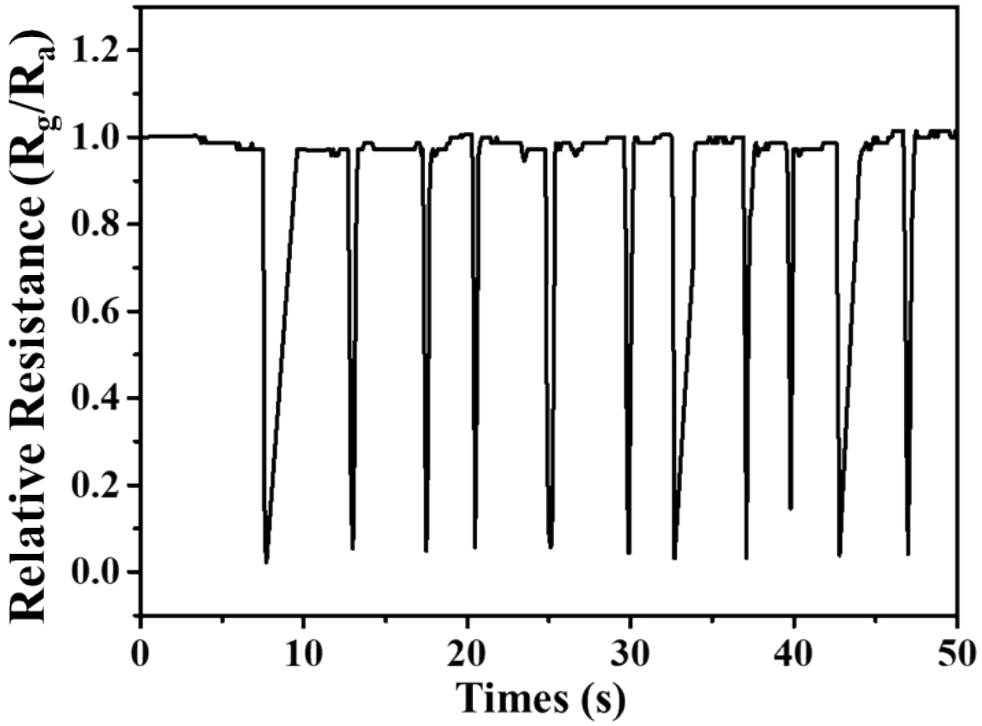

Figure S12. Dynamic response of textile-based sensor for respiratory monitoring after placing 10 weeks.

Even after a long-time placement, the senor also presents excellent sensitivity and stability.

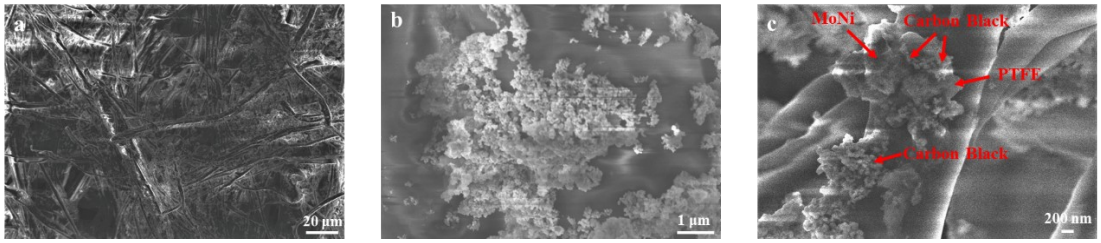

Figure S13. SEM images of the textile-based temperature sensor with different magnifications.

Table S1. DFT calculation of lattice parameters for $MoNi_4$ and WNi_4

State / Lattice parameters		Before relaxation	After relaxation
$MoNi_4$	a (Å)	5.720	5.736
	b (Å)	5.720	5.736
	c (Å)	3.564	3.573
WNi_4	a (Å)	5.730	5.737
	b (Å)	5.730	5.737
	c (Å)	5.730	3.583

DFT calculation shows that the changing range of lattice volume for $MoNi_4$ and WNi_4 is different. The change of WNi_4 is higher than $MoNi_4$, indicating the lower order degree of the lattice. According to research, the order degree of the lattice is related to the lattice defect. Therefore, the more lattice defect makes WNi_4 higher resistance as compared with $MoNi_4$.

Humidity influence

When the sensor is used at room temperature, the moisture from breath can be adsorbed on the surface of the sensing layer and cause resistance change. Such effect can change with humidity until the sensing layer surface forms a continuous water layer. Room temperature testing result as shown in Figure S11, the researcher continuously blows into the sensor, and the resistance is unable to recover to the initial value at first. After blowing several times, the resistance can recovery to a stable value, which indicates the sensing layer surface forms a continuous water layer and the whole system reaches a steady state. Nevertheless, the humidity influence can be eliminated in the textile-based sensor which is fabricated in our experiment.

At high working temperatures of 230 and 330 ℃, the influence of breathing moisture for resistance could be neglected, because the water is not easy to be adsorbed on the sensor surface. Owing to the little effect of humidity on resistance change, we analyze the sensor performance mainly focusing on temperature variation.

Temperature sensitivity enhancement mechanism

Due to the atom radius difference of Mo/W and Ni, the diffusion of atoms could cause internal stress that deforms the lattice, leading to lattice distortion. Such distortion sites are distributed in the lattice interior, and act as the trap to restrict surrounding electron motion. The enhancement of temperature and voltage can cause relaxation and decrease lattice defect degree, which promotes the movement of electrons. According to the DTF calculation results, there are electrons hybridization between Mo/W and Ni. For example, the electrons of s, p and d orbit in Mo and the s, p, and d orbit in Ni can form the s-p and s-d hybrid, which reveals the conductive mechanism of $MoNi_4$ and WNi_4. Due to the special electronic structure of transition metals, the d band is narrower and the effective quality of electron is high, and thus the electric conduction mainly relies on the electrons of the s band. Therefore, the chances of electron scattering into the d band are greatly enhanced, making $MoNi_4$ and WNi_4 a high resistance. Besides, a significant number of defects also play the role of electron scattering.

Compared with the lattice constants of $MoNi_4$ and WNi_4 before and after relaxation, the lattice constant of WNi_4 presents a higher change range (Table S1). This is due to the larger atom radius difference between the W and Ni than Mo and Ni, thus causing the bigger internal stress, which makes WNi_4 higher resistance. Meanwhile, there are more defects that exist in the WNi_4 lattice, and the higher scattering probability also contributes to the high resistance. These reasons explain why the WNi_4 (6.5-8 GΩ) resistance is higher than $MoNi_4$ (3.5-5.5 GΩ).

There are many reasons that can explain the temperature sensitivity difference

between WNi_4 and $MoNi_4$, such as phonon/electron free path theory, phonon-electron coupling theory, charge transfer resistance, and so on. According to the above discussion, we know that the lattice volume change of WNi_4 is higher than $MoNi_4$ when comparing their lattice parameters before and after relaxation, which indicates longer free path could exist in WNi_4. On the basis of heat conduction theory, heat transfer is related to the interaction within the phonon-phonon and phonon-lattice, and therefore the longer free path indicates more time for heat conduction. Generally, these theories explained the root cause of high resistance and the difference of temperature sensitivity between WNi_4 and $MoNi_4$, and the testing results also proved the above theories.

Testing results demonstrate the electron-detrapped traps model, and the B-value (or E_a) slightly decreases with measurement voltage (Figure S10). This is attributed to a high voltage that could promote electrons within the traps to migrate away easier.

References

1 Duan, Y.; Yu, Z. Y.; Yang, L.; Zheng, L. R.; Zhang, C. T.; Yang, X. T.; Gao, F. Y.; Zhang, X. L.; Yu, X. X.; Liu, R.; Ding, H. H.; Gu, C.; Zheng, X. S.; Shi, L.; Jiang, J.; Zhu, J. F.; Gao, M. R.; Yu, S. H. *Nat. Commun*. 2020, **11**, 4789.

2 Sheng, W. C.; Bivens, A. P.; Myint, M. Zhuang, Z. B.; Forest, R. V.; Fang, Q. R.; Chen, J. G. G.; Yan, Y. S. *Energy Environ. Sci*. 2014, **7**, 1719–1724.

3 Zhang, J.; Wang, T.; Liu, P.; Liao, Z. Q.; Liu, S. H.; Zhuang, X. D.; Chen, M. W.; Zschech, E.; Feng, X. L. *Nat. Commun*. 2017, **8**, 15437.

4 Wang, W. Y.; Wang, G. C. *J. Phys. Chem. C*. 2021, **125**, 18653–18664